ingegneria sismica
International Journal of Earthquake Engineering
Anno XLIII - Num. 1 - 2026

Multi-Intelligent Body Collaborative Decision Making and Control Mechanism in Intelligent Inspection Systems

Yutian Wang[1,2,*]

[1] School of Electrical Engineering, Beijing Jiaotong University, Beijing, 100044, China
[2] Guoneng Guohua (Beijing) Cogeneration Power Co., Ltd., Beijing, 100018, China

SUMMARY: *This thesis concentrates on the collaborative decision-making and control between several intelligent agents in an intelligent inspection system. It mostly explores cooperative target detection and obstacle avoidance routing plans of multi-agent systems. Cooperative target detection method has adopted YOLOv3 as its core network and combines double-threshold decision-making with D-S evidence theory to improve detection probability. Obstacle avoidance planning method alters the artificial potential field method so that the inspection robot is able to independently perform obstacle avoidance. Results of experiments prove that the mAP of the cooperative target detection algorithm is higher than the original algorithm by 0.6-10.2, or 0.733, indicating that it is possible to accurately identify various types of targets. The mean length of the routes produced by the obstacle-avoidance path planning algorithm is 24 grids, implying that the robot can navigate and evade obstacles efficiently. The model suggested in this paper allows recognizing the object to avoid and the planning of the obstacle-avoidance path, thus promoting collaborative decision-making and coordinated control of several intelligent agents in smart inspection situations.*

KEYWORDS: *YOLOv3; target detection; artificial potential field method; obstacle avoidance path planning; intelligent inspection system*

1 Introduction

As an advanced aerial equipment, UAVs are attracting more and more attention due to their excellent operational capabilities in complex and dangerous environments [1]. Due to its ability to flexibly respond to the needs of line inspection in complex terrain and changing environments, UAVs are gradually becoming an important tool for intelligent inspection [2]. However, when performing inspection tasks, UAVs often face a low-altitude flight environment with dense obstacles and complex paths, and at the same time, due to the increased demand of society for inspection tasks, the robustness and stability of single intelligences under complex tasks have certain limitations. At this time, the advantages of multi-intelligent body system can be fully realized. In fact, the research on multi-agent systems is driven by collective phenomena that take place in nature like swarms of fish, birds flying together, colonies of ants, and similar group phenomena [3]. Unlike a single intelligent agent, multi-agent systems can harness the advantages of teamwork and coordination, and the system redundancy increased by its scale expansion can still rely on other intelligent bodies to continue the inspection task when some of them fail, which enhances the robust performance of the inspection operation [4, 5].

*YutianWang1989@163.com
https://doi.org/10.65102/is2026483
Published: 30 April, 2026

Collaborative control algorithms for multiple intelligences, which focuses on how to coordinate their behaviors and relationships among multiple intelligences to accomplish tasks cooperatively, efficiently, and conflict-free [6]. Inspired by the cluster behavior exhibited by organisms in nature in the early days, researchers in related fields have also achieved a large number of research results in multi-intelligent body cooperative control. However, since classical control methods need to rely on accurate model and environment information, which are difficult to obtain in real-world environments, and the design and construction of strategies require a large amount of relevant expertise [7, 8]. As a result, the performance of traditional control algorithms tends to decrease dramatically even in the case of disturbances and changes in the environment, and their adaptability in the actual working environment is difficult to ensure [9].

For the optimization of multi-intelligent body cooperative control, some scholars have studied it from the perspective of consistency. Coherent control is a collaborative approach for multi-intelligent systems to achieve convergence of states or behaviors of all intelligences through local information interactions, the core of which lies in the design of distributed rules, so that each intelligence only relies on the information of its neighboring nodes to adjust its own dynamics, and ultimately, the entire system converges to a common goal state without the need for centralized commands [10]. This process relies on mathematical protocols to ensure that the system self-organizes and coordinates in a dynamic environment, essentially transforming local interactions into global consistency and providing a foundational framework for multi-intelligence collaboration [11]. For example, Qin, J et al [12] investigated group coherence for single integrator type multi-intelligent systems with disturbances, where external perturbations are modeled indeterministically, and thus they demonstrated that the intelligent systems are capable of achieving group coherence based on the structure and strength of the coupling between the intelligences. Rehman, A et al [13] reformulated the Lipschitz nonlinear and adaptive protocols in intelligent body dynamics using a composite linear parameter approach for homogeneous nonlinear multiintelligent body systems with bounded disturbances under an undirected connected graph, proposed robust nonlinear adaptive consistency protocols based on edges and verified the consistency of multiintelligent bodies. Dong, Y and Huang, J [14] investigated the leader-follower coherence problem for multi-intelligent body systems with perturbations, and designed a cooperative control algorithm that does not depend on the system velocity, realizes position feedback control and constructs a bounded control law based on bounded potential functions to ensure that the system connectivity is maintained. Tran, V proposed a distributed multi-intelligent body system control framework based on feedback consistency and applied it to the UAV cooperative handling system to realize the UAV formation keeping tracking control under the effect of suspended load perturbation [15].

In collaborative control systems, physical constraints are intrinsic limitations embedded in the physical characteristics and operation logic of the system, which are rooted in the unbreakability of hardware performance boundaries, heterogeneous architectural differences, and resource provisioning capabilities [16]. These limitations cannot be directly eliminated or ignored in collaborative control problems, but need to be circumvented or compensated by appropriately designing control strategies. For example, Li, Z et al.analyzed the distributed optimal coordination problem of heterogeneous linear multi-agent systems with the help of an event-triggered approach. The main characteristic of their analysis is that the local gradient follows the property of unknown Lipschitz constant and known convexity constant. Then, the authors proposed a fully distributed control scheme for coordinating all agents into the optimal coordinated state with the minimized value of the global objective function [17]. Yu, J et al. broadened the control framework of Kajoie multi-agent systems from spatial

collaborative control to the co-scheduling process of these systems by studying the formation problem under time-varying conditions. Specifically, the researchers suggested the adaptive, practically optimal time-varying formation tracking protocol [18]. The next study focuses on the formation tracking control problem for multi-robot systems with incomplete information. Li, Y. et al. formulated a decentralized adaptive fault-tolerant control approach combining fuzzy logic approximation, adaptive backstepping design and predefined performance limits to provide fault-tolerant time-varying formation trajectory tracking [19]. Jia, Y and Zhang, W considered the issue of the formation control problem for the multi-agent systems located in the 3D environment within the pilot-follower approach. Thus, the researchers proposed a novel distributed algorithm according to the nearest-neighbor interaction rule allowing all the agents to converge to the same speed and reach the required formation [20]. In order to solve the problem of topological uncertainties in cooperative control, Chen, Y. et al. used fuzzy modeling technique to create the adaptive approximation method. The main idea of this technique is to represent the topology uncertainty using fuzzy rules and exploit the features of time-varying topology [21].

In addition to the physical constraints, the communication network, playing the role of the information nerve of a multi-agent system can be also affected by dynamic constraints including time-varying topology and network attacks. Such restrictions might lead to a mismatch between control strategies due to the fact that they are limiting information exchange between agents, thus negatively affecting the collaborative effect, in general. Multi-agent systems in dynamic network settings Researchers have conducted in-depth research on these concerns to enhance the stability and security of multi-agent systems in dynamic network settings. As an example, Zhang, S et al. investigated the observer-based event-triggered robust and secure synchronization control problem of multi-agent systems subject to spurious data injection attacks under directed graphs. They proposed a novel event-triggered mechanism based on state estimation thresholds using Bernoulli processes to model false data injection attacks that occur spontaneously within sensor-to-controller and controller-to-actuator transmission channels [22]. The CommNet algorithm proposed by Sukhbaatar, S and Fergus, R establishes a transmission channel between the intelligences in a MAS to realize a multi-intelligence control system with state information interaction, in which the communication ranges of the intelligences within the system are freely chosen to achieve free communication throughout the control process with an equal-step communication frequency [23]. Wang, Y et al. combined the multi-intelligence body bifurcation consensus theory with heading dynamic system modeling to propose a virtual hierarchical bifurcation control strategy, which utilizes the virtual hierarchical structure to coordinate the intra- and inter-layer interactions, so that the formation can reach the bifurcation consensus even when there is a signal delay and strictly maintain the formation shape [24]. Yang, X, on the other hand, considered heterogeneous multi-intelligent body systems with different parameter matrices, which reduces the difficulty of analyzing heterogeneous systems by constructing augmented closed-loop systems containing all the intelligences. It is noted that heterogeneous multi-intelligent body systems consisting of different types of intelligences are more general and practical cases [25]. Z et al. Feng have studied the robust connectivity-preserving rendezvous problem of second-order multi-agent systems with non-linear dynamics and disturbances that are not known. They suggested a distributed control law using the gradient of the potential function that preserves connectivity between the agents and provides rendezvous control [26].

Reinforcement learning works by continuously interacting with the environment. It evaluates the value of the action being performed in terms of its reward function and instructs the agent to adopt strategies for maximizing rewards in their explorations. Sun, L. et al.

created a reinforcement learning approach for multi-tasking and migration using a parameter combination technique. This model enables simultaneous optimization of many tasks via parameter combination, while also supporting sharing and migration among tasks via the same approach. This allows agents to learn effectively across various tasks and avoid task interference [27]. Chen, C. et al. designed a policy learning technique for reinforcement learning based on output feedback. By combining robust output regulation with reinforcement learning, it creates a distributed robust optimal synchronization process of heterogeneous multi-agent systems without the need for detailed knowledge about the underlying dynamics of such systems. The algorithm requires only input and output data from neighboring nodes [28]. Van Der Pol, E. undertook a quantitative experimental investigation into common technical traits associated with multi-agent reinforcement learning approaches for signal control applications. He presents guidelines for choosing baseline performance metrics for designing intelligent agents [29]. Foerster, J. et al. have created a multi-agent reinforcement learning algorithm called COMA with a centralized value assessment network. Centralized critics provide instructions for learning strategies, which are then implemented in a discrete action space [30]. Hu, S et al. proposed Updet, a generalized multi-agent reinforcement learning model based on Transformer architecture. In the model, individual policies are separated from the environment via mean policy decoupling, allowing each agent to operate independently without relying on other agents [31].

In the process of multi-agent collaborative decision update, the problem of opposite directions of decision gradient update due to the switching between tasks has always existed. To alleviate the gradient conflict problem in the multi-task training process, Lowe, R et al. extended the DDPG algorithm to the multi-agent domain based on the CTDE framework. The proposed MADDPG algorithm effectively alleviates the problem of difficult convergence of strategies caused by unsteady environments for multi-agents, and this algorithm can adapt to both cooperative and competitive environments [32]. Setter, T and Egerstedt, M In order to minimize the overall energy depletion of multi-intelligentsia cooperative motion, an energy-constrained control strategy is proposed for coordinated motion control of multiple robots, which allows the robots to complete the rendezvous in the shortest possible time [33]. Shen, Z et al. In order to introduce saturation constraints into the optimization problem, they designed a new local cost function based on hyperbolic function, proposed a new iterative algorithm for saturated input strategy, and constructed a multi-intelligence body control framework based on actor-critic architecture to implement the algorithm [34]. Fei, Y et al. considered a parameter heterogeneous multi-intelligent body system caused by model uncertainty, and in order to estimate the uncertainty of the system, a three-layer neural network observer was constructed and a collaborative weight adjustment process fully related to the local error was proposed for adaptive estimation of uncertainty in finite time [35]. By combing through the existing approaches, it is found that the problem of multi-intelligent body cooperative control under non-ideal conditions has received extensive attention, and scholars have proposed many enlightening solutions for the constraints of limited on-board resources, time-varying network topology, random attacks, etc., which further improve the application potential of multi-intelligent body cooperative control. However, most of the existing researches focus on ensuring the feasibility of collaboration under constraints, and in order to ensure that the smart inspection can fully meet the actual needs of inspection tasks, further improvement of the collaboration performance under constraints is needed, and further in-depth explorations are urgently needed.

The intelligent inspection system elements are given in this paper. YOLOv3 is chosen to be used as the fundamental detection and recognition algorithm when making cooperative target detection decisions with more than one agent. Once everything has been summed up, it

undergoes the double-threshold decision module and the probability correction module (based on D-S evidence theory) and finally out come the results of cooperative detection. To control the inspection robot in terms of obstacle avoidance, the artificial potential field algorithm is optimized. The dead-zone distance is described, and effective dynamic obstacle-avoidance control of the robot can be obtained by computing the obstacle, the angle between the robot and the target location, and the distance between the obstacle and the boundary. The detection capabilities of the cooperative target detection algorithm are tested with a publicly available dataset and the path-planning capabilities of the developed approach are evaluated by means of raster maps and real-life experiments. The cooperative target detection algorithm and obstacle-avoidance path planning approach developed in this work can assist in the operation and maintenance activities of intelligent inspection systems and offer technical assistance to scientific operation and maintenance.

2 Intelligent inspection system

Inspection is the main means to ensure the normal operation of equipment, intelligent inspection utilizes artificial intelligence, Internet of Things, big data and other technical means to carry out all-round and efficient supervision and inspection of relevant equipment and facilities, which can realize the automatic recording and analysis of various data. Intelligent inspection system is mainly composed of remote client, local server and hardware equipment.

2.1 Remote Client

Remote client consists of enterprise private network, operation and maintenance client and display big screen. The remote client can log in the remote browser, can view the inspection process data and images, inspection record table, alarm record, maintenance basic information, set/query the operating line parameters, set/query the target preset point parameters, update the maintenance map information, query the operating status of the operation robot, etc., and can generate analysis reports.

2.2 Local servers

The local server consists of data/image server, database, APN security terminal, switch and so on.

(1) The data/image server is embedded with AI processing unit, through the graphic processing algorithm running on the high-speed GPU, according to the state of the execution task, real-time on-line intelligent analysis image analysis of the equipment working status, instrument pointer, switch status, foreign object encroachment limit, and output the analysis results and judgment of the alarm status information.

(2) The database is deployed in the data/graphics server, which is used to store inspection task parameters, inspection process data, alarm records and historical videos. The server adopts a top-shelf industrial control chassis, and the processor selects Intel i9 CPU with a main frequency of 3.7 GHz, no less than 64 GB of RAM, no less than 1 TB of solid-state disk, no less than 16 TB of mechanical hard disk, no less than 2 Gigabit network ports, an independent GPU graphic card, and RAID arrays.

(3) APN security terminal is the only channel connecting to the enterprise private network and is responsible for transmitting the inspection process data, alarm records, and real-time video to the enterprise private network for viewing by remote clients.

2.3 Hardware

The hardware equipment consists of inspection robot, guide rail, adapter box and wired private network. The inspection robot utilizes precise displacement control, sliding contact power supply, DC broadband carrier, thermal imaging acquisition, wireless radio frequency, ultrasonic ranging, remote control, TTS text-to-speech and other technologies to realize precise target-pointing cruise, high-definition image acquisition, and high-speed data transmission. The whole machine is easy to maintain and suitable for indoor inspection in industrial occasions.

3 Multi-intelligence body collaborative decision-making and control mechanism

Based on the intelligent inspection system, its multi-intelligent body collaborative decision-making and control mechanism is analyzed, the multi-intelligent body collaborative target detection and recognition algorithm is proposed to assist the decision-making of the intelligent inspection system, and the inspection robot obstacle avoidance path planning algorithm is proposed to realize the control of the inspection robot.

3.1 Collaborative Target Detection Algorithm

3.1.1 Algorithmic framework

Multi-intelligent body collaborative decision-making is to give globally optimal guidance by comprehensively considering the final detection and recognition results output by each intelligent body. The framework of multi-intelligence body collaborative decision-making is shown in Fig. 1, and the input of the collaborative target detection module is the target detection result (including target location and probability) of a single intelligent body, and the output is the globally optimal detection result after collaborative processing (more complete information and higher accuracy). The collaborative detection and recognition problem is divided into single-intelligent body target detection algorithm, information summarization module, dual-threshold determination module and probability correction module.

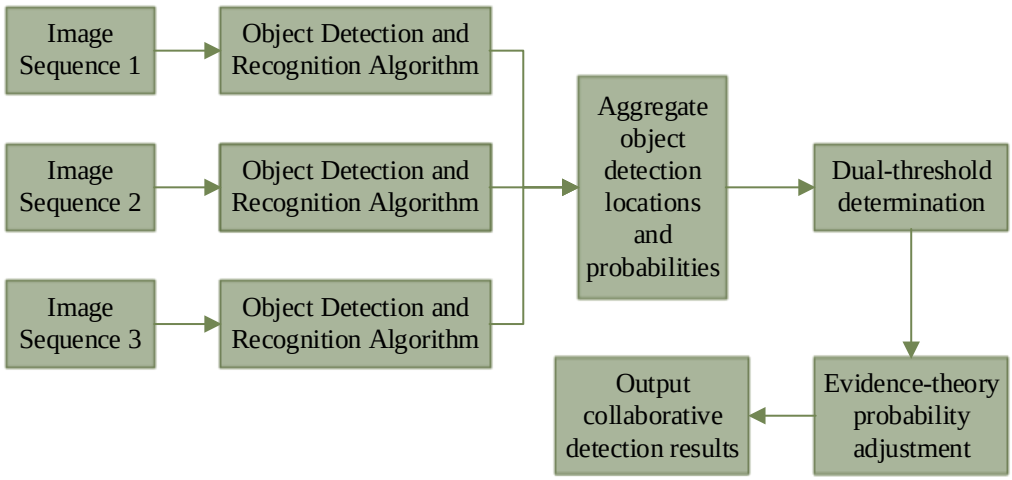

Figure 1: The multi-smart association decision framework

3.1.2 YOLO V3 algorithm

In this paper, YOLO V3 is used as the basic detection and recognition algorithm.The YOLOv3 network structure mainly consists of three parts: backbone network, multi-scale feature extraction network and detection network.

The backbone network adopts the Darknet53 network which does not contain a fully connected layer, because of its deeper network structure and richer number of parameters, it has better feature extraction capability than Darknet19 used in YOLOv2, and it is also better than the lightweight networks such as MoblieNet, etc. Darknet53 backbone network firstly performs the conventional 3×3 convolution operation on the input features, and then superimposes five multi-scale features on each of them, and then the input features are converted into the MoblieNet. The Darknet53 backbone network first performs a conventional 3×3 convolution operation on the input features, and then superimposes five residual networks, which contain “1, 2, 8, 8, 4” residual blocks in turn. darknet53's downsampling process abandons the maximal pooling, and instead employs a convolution operation with a step size of 2, which avoids the loss of features brought by pooling operations. A total of five downsampling operations are performed in the backbone network, and each downsampling reduces the feature map size by half. Each of the 23 residual network structures contained in the residual block consists of 1 × 1 and 3 × 3 convolution operations. Of these, the 3 × 3 convolution is the primary means of extracting features, and the 1 × 1 convolution is primarily used to adjust the number of channels. The two convolutions are superimposed on each other to create a deeper network structure, which can effectively avoid the explosion and dispersion of gradient information while enhancing the feature extraction capability of the network.

Although a large number of residual network structures are stacked in the Darknet53 backbone network, the calculation is not complicated, and the residual network used in Darknet53 can be expressed by the following equation:

$$X_1 = \sigma\left\{\beta\left(W_1, X\right)\right\} \tag{1}$$

$$X_2 = \sigma\left\{\beta\left(W_2, X_1\right)\right\} \tag{2}$$

$$X_3 = X + X_2 \tag{3}$$

where X denotes the input features of the residual structure, $\left(W_1, X\right)$ denotes that the input features are subjected to a convolution operation with weights W_1, where the convolution kernel of W_1 has a size of 1×1, β denotes the batch normalization operation, σ denotes Relu nonlinear activation. $\left(W_2, X_1\right)$ denotes that the input features are subjected to a convolution operation with weights W_2, where the convolution kernel size of W_2 is 3×3, X_2 denotes the backbone output features of the residual structure, and X_3 denotes the final output features of the residual structure .

As far as the multi-scale feature fusion network construction is concerned, the section in question primarily discusses the design concept based on the FPN. The multi-scale feature fusion network combines the feature information of various resolutions by using the outputs of the 3rd, 4th, and 5th residual networks as its input features. Next, the network uses convolution kernels of size 1x1 and 3x3 and up-samples the small-scale feature maps to perform multi-scale feature fusion. The YOLOv3 detection network produces feature maps at three scales: 13 x 13, 26 x 26 and 52 x 52, which can be used to detect objects of any size.

3.1.3 Information summarization module

The role of information summarization is to unify the information of multiple intelligences under the same spatio-temporal coordinate system after processing, to accelerate the detection speed and increase the detection range through parallel work of multiple machines. For targets with consistent spatio-temporal coordinates, the detection results or classification results are sent to the subsequent module for further processing. For candidate targets with one inconsistent temporal and spatial coordinates, the original detection and identification results are retained and added to the global posture. The mathematical tools for information aggregation are coordinate transformation and linear interpolation.

3.1.4 Dual-threshold decision module

The role of the dual-threshold determination module is to maximize the detection rate and reduce the false alarm rate by utilizing the observation conclusions of multiple intelligences on the same target under different viewpoints. The specific steps for filtering the preliminary summarized detection and recognition results using two different thresholds, high and low, for detection are as follows:

Target detection is performed for each viewpoint image using the lower threshold, and a candidate target is considered to be a real target if it is detected at a certain viewpoint with a confidence level greater than the high threshold and is also detected at other viewpoints. If a candidate target is detected with a confidence level greater than a high threshold in one viewpoint but is not detected in all other viewpoints, it is considered to be a suspected target and is labeled to wait for the next round of detection cycle to be performed again. If the candidate target does not have a high threshold of confidence for detection under all viewpoints, the target is considered a false alarm. All targets except false alarm targets require probability correction using evidence theory.

3.1.5 Probability correction module

The role of probability correction is to fuse the detection probability values or recognition confidence given by different intelligences into a more accurate and trustworthy value, and D-S evidence theory is used here as a tool for fusion.

The D-S evidence theory outlines a number of important terms such as hypothesis space, focal element, confidence function, and likelihood function. Hypothesis space can be described as the set of all conceivable judgments that have an overlap, either partial or complete. The confidence function, also known as the lower-bound function, is the cumulative probability of a set of hypotheses. Likelihood function, alternatively referred to as upper-bound function, is the combination of probabilities of the events that intersect with a certain hypothesis. The particular fusion rules are given below:

θ is the hypothesis space, and the mass function is a basic probability distribution function m over the hypothesis space that satisfies:

$$m(\theta) = 0, \sum_{A \subseteq \theta} m(A) = 1 \tag{4}$$

For any A belonging to θ, the Dempster synthesis rule for two mass functions m_1, m_2 on θ is:

$$m_1 \oplus m_2(A) = \frac{1}{K} \sum_{B \cap C = A} m_1(B) \cdot m_2(C), B, C \subseteq \theta$$
$$K = 1 - \sum_{B \cap C = \varnothing} m_1(B) \cdot m_2(C) \tag{5}$$

For any A belonging to θ, the Dempster synthesis rule for n mass functions $m_1, m_2, \cdots, m_n$ on θ is:

$$(m_1 \oplus m_2 \oplus \cdots \oplus m_n)(A) = \frac{1}{K} \sum_{\substack{A_1 \cap A_2 \cap \ldots \cap A_n = A \\ A_1, A_2, \ldots, A_n \subseteq \theta}} m_1(A_1) \cdot m_2(A_2) \cdots m_n(A_n)$$
$$K = 1 - \sum m_1(A_1) \cdot m_2(A_2) \cdots m_n(A_n) \tag{6}$$

3.2 Obstacle avoidance path planning algorithm

In this paper, the artificial potential field method is used for robot obstacle avoidance planning and control in order to quickly establish an autonomous obstacle avoidance system for inspection robots.

3.2.1 Artificial potential field method

The artificial potential field method (APF) for robot path planning and obstacle avoidance is based on the force of the mobile robot in the artificial potential field for planning, the force of the robot in the artificial potential field is shown in Fig. 2.

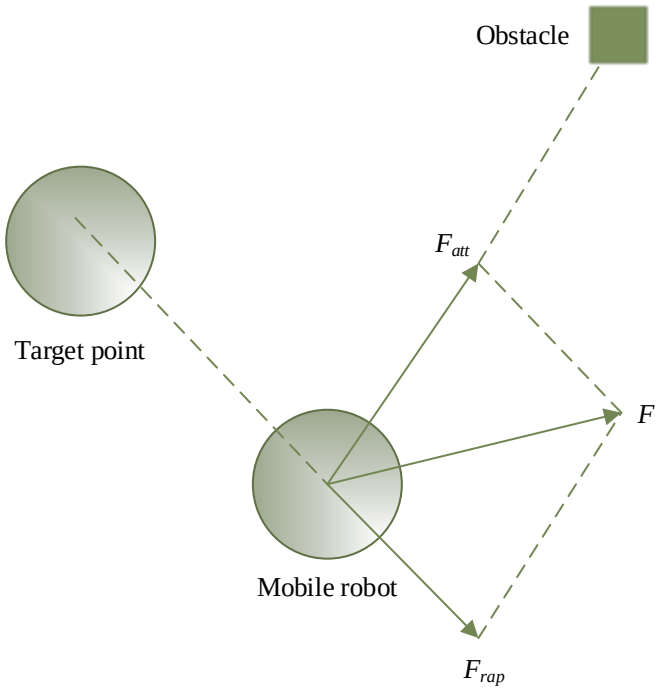

Figure 2: The force of the robot in the artificial potential field

The specific realization method is as follows: first of all, an artificial virtual potential field is constructed in the space of the operating environment of the mobile robot, which consists of two parts: (1) the gravitational potential field U_{att} generated by the target point on the mobile

robot, which generates the gravitational force F_{att}, whose direction is pointing to the target point from the robot. (2) A repulsive potential field U_{rep} generated by an obstacle on the mobile robot, which generates a repulsive force F_{rep} in the direction from the obstacle to the robot. The total potential field in the running space is the superposition of the repulsive and gravitational fields. Thus, the movement of the mobile robot is controlled by the combined force F of the gravitational force F_{att} and the repulsive force F_{rep}.

The gravitational potential field function U_{att} and the gravitational force F_{att} are:

$$U_{att}(x) = k\left\|x - x_g\right\|^2 \Big/ 2 \tag{7}$$

$$F_{att}(x) = -grad\left[U_{att}(x)\right] = -k\left\|x - x_g\right\| \tag{8}$$

The repulsive potential field function U_{rep} and the repulsive force F_{rep} are expressed as:

$$U_{rep} = \begin{cases} p/2*(1/d - 1/d_0)^2, & d < d_0 \\ 0, & d \geq d_0 \end{cases} \tag{9}$$

$$F_{rep}(x) = -grad\left[U_0(x)\right] = \begin{cases} p/d^2*(1/d - 1/d_0) & d < d_0 \\ 0 & d \geq d_0 \end{cases} \tag{10}$$

where k is the positive proportionality gain coefficient of the gravitational potential field, $\left\|x - x_g\right\|$ is the relative distance between the robot and the target point, p is the proportionality gain coefficient of the repulsive field, d is the distance between the robot and the obstacle, and d_0 is the distance threshold at which the repulsive potential field will have an effect on the robot, i.e., the radius of the radius of action of the influence.

According to the repulsive potential field, gravitational potential field, repulsive force and gravitational force, the total situation field function $U(x)$ and the combined force F can be obtained as:

$$U(x) = U_{att}(x) + U_{rep}(x) \tag{11}$$

$$F(x) = F_{att}(x) + F_{rep}(x) \tag{12}$$

Once you get the combined force, split the combined force into horizontal x and y components and do the trigonometry to get the actual direction you should be going.

3.2.2 Improvement of the artificial potential field method

Conventional artificial potential field techniques usually have local minima. The number of obstacle points that will be achieved in real-time map construction is bounded due to the fact that the depth camera has a limited field-of-view range in robots obstacle avoidance. At the same time, as all obstacles registered by the camera are located before the camera, the robot may easily end up in a local-minimum condition when estimating the overall potential field.

This problem can be solved by changing the original algorithm by marking a small region surrounding the obstructed region as the dead-center distance. The robot automatically enters the dead center once it comes within this zone. Now the midpoint of the detected obstacle is used as the center of the obstacle. Next, the angle between the coordinate system of the obstacle center and the coordinate system of the target point, the angle between the obstacle center and the obstacle itself, and the distance between the obstacle and the boundary is computed. Depending on the values of these two angles and the distance to the border, the robot is directed to rotate through some angle until it gets out of the dead-center zone. In case of not moving out prior to the boundary, the robot keeps rotating at a constant angle. In case of being unable to leave the dead-distance range even when reaching the boundary, the robot reverses its movement until leaving that range or going to another boundary. This means that in such an instance the position is considered as a dead end and the robot halts its motion and so achieves independent obstacle avoidance.

Let the dead distance to the obstacle be d_0, the true distance to the obstacle be d, the safe distance to the boundary be d_s, the actual distance from the boundary be d_t, the coordinates of the target point be (X,Y), the coordinates of the center point of the current obstacle be (x_0,y_0), and the current coordinates of the body be (x,y). Then from $\theta=\arctan\left(\frac{Y-y}{X-x}\right)$, the angle between the machine body and the target point and the angle between the obstacle center point and the target point can be found as θ_1,θ_2, respectively.

Through the detection of obstacles in the robot environment, and then use the artificial potential field method to realize the robot's autonomous walking and obstacle avoidance. Figure 3 shows the robot combined with the obstacle target detection and obstacle avoidance process, first of all, the confirmation of the target area, and at the same time calculate the gravitational force of the target area on the robot. Obstacle target detection is performed using the YOLOv3 target detection algorithm on the acquired image information, and the distance of the obstacle is acquired according to the detection result, while the size of the obstacle and the coordinate value under the camera coordinate system are acquired under the set threshold. According to the acquired obstacle results, coordinate transformation is performed and the obstacle repulsion is calculated at the same time. Using the gravitational force and the repulsive force to calculate the combined force, calculate the coordinates of the next position according to the combined force result and the step size, and update all the coordinates continuously, and control the robot to walk to the target area in the shortest path to avoid the obstacles.

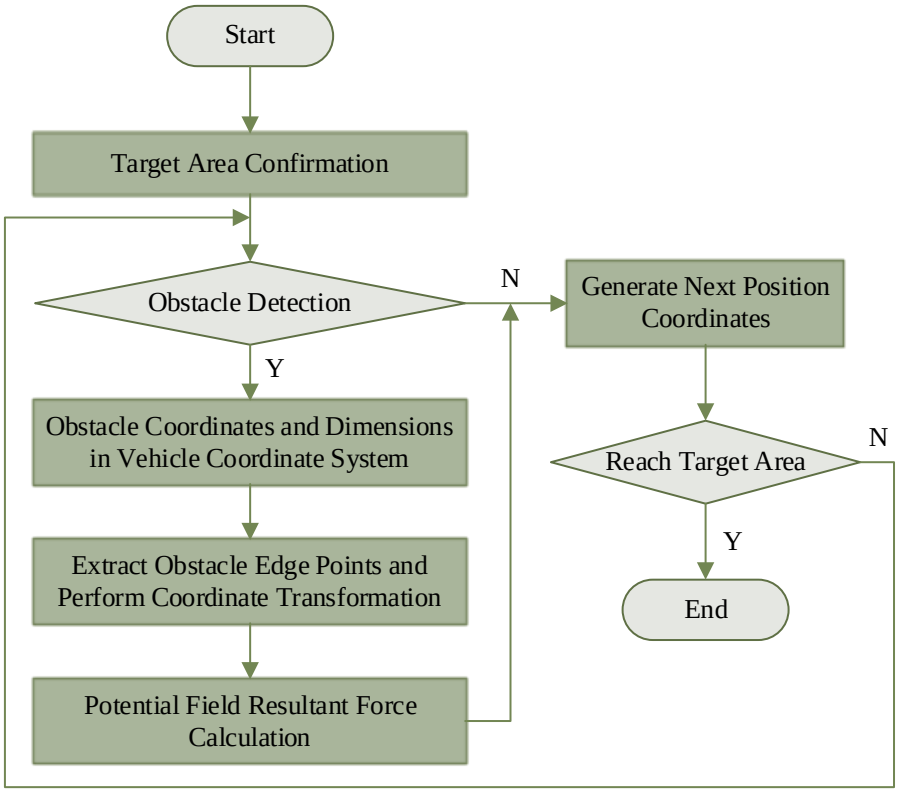

Figure 3: Robot avoidance process

4 Experiments and analysis of results

4.1 Collaborative target detection analysis

4.1.1 Introduction to the data set

This section performs experimentation on a publicly available dataset. The chosen dataset in the present study is the Udacity dataset that has been mostly used to measure how well the model detects things. A Point Grey research camera was used to capture the Udacity Autopilot dataset with a resolution of 1920 x 1200. Its first sub-dataset consists of daytime data acquired within Mountain View, California and neighboring cities. It comprises of 9, 423 frames and over 65, 000 labeled objects. The annotation is done both by machines and human beings, and the object categories are vehicles and trucks and people. The second sub-dataset is significantly larger than the first, where the number of frames rises to 15, 000, and every label is filled in by hand.

Udacity dataset is split into training, testing, and validation sets with a ratio of 6:2:2. The measurement indicators are mean average precision (mAP), precision, recall and F1 score.

4.1.2 Experimental results

The experiments are conducted on the Udacity dataset which includes these 11 categories: car, pedestrian, trafficLight-Red, trafficLight-Green, truck, trafficLight, biker, trafficLight-RedLeft, trafficLight-GreenLeft, trafficLight-Yellow, and trafficLight-YellowLeft.

The chosen benchmark in the experimental comparison is a collaborative target detection algorithm previously described. Table 1 is the comparison between the collaborative target detection algorithm and other popular target detection algorithms based on the Udacity dataset.

Test results of other algorithms on this dataset are also used as comparative references. Typical target detection algorithms with the highest mAP are most widely used, but the proposed collaborative target detection algorithm has the highest mAP value of 0.733, which is higher than any other method compared. Its development varies between 0.6% and 10.2% indicating that the developed collaborative target detection algorithm performs better than the other methods in terms of target detection.

Table 1: Effects of different detection algorithms on Udacity data sets

Detection algorithm	Backbone network	mAP (IoU=0.5)
SSD-VGG16	VGG16	0.631
Faster R-CNN-ResNet50	ResNet50	0.652
RetinaNet-ResNet50	ResNet-50	0.683
FCOS-ResNet50	ResNet-50	0.665
TridentNet-ResNet50	ResNet-50	0.727
CornerNet-Hourglass104	Hourglass104	0.667
Ours	DarkNet53	0.733

Each category in the Udacity validation set and test set is tested separately and the results are shown in Fig. 4 and Fig. 5. On the Udacity test set and validation set, the results of this paper's collaborative target detection algorithm for each category are concentrated between 0.63 and 0.76, and the proposed algorithm achieves good results on the Udacity dataset, which can well detect targets of different categories and morphologies.

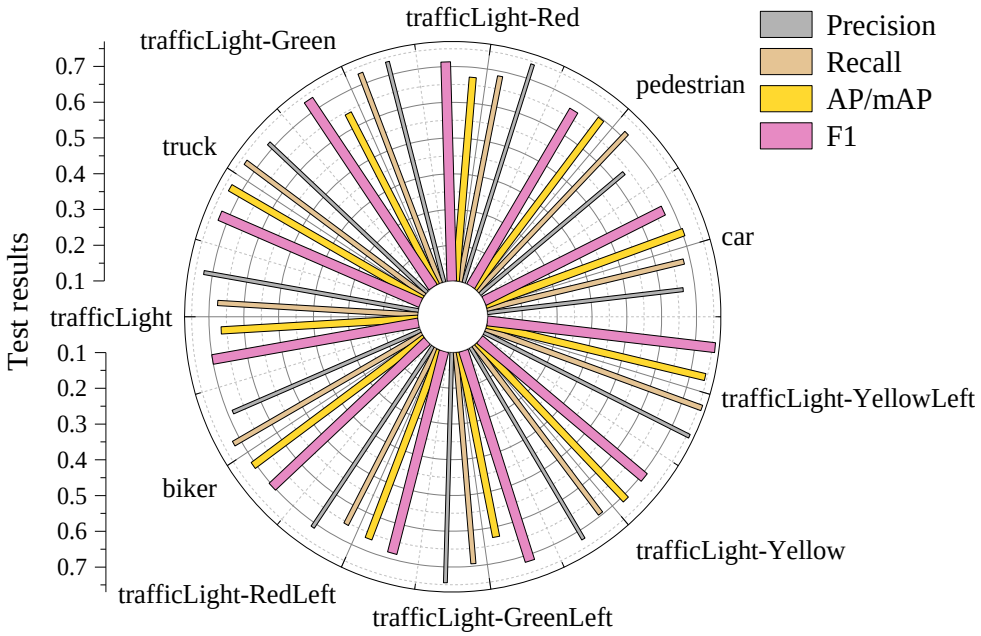

Figure 4: Different category test results in the Udacity test set

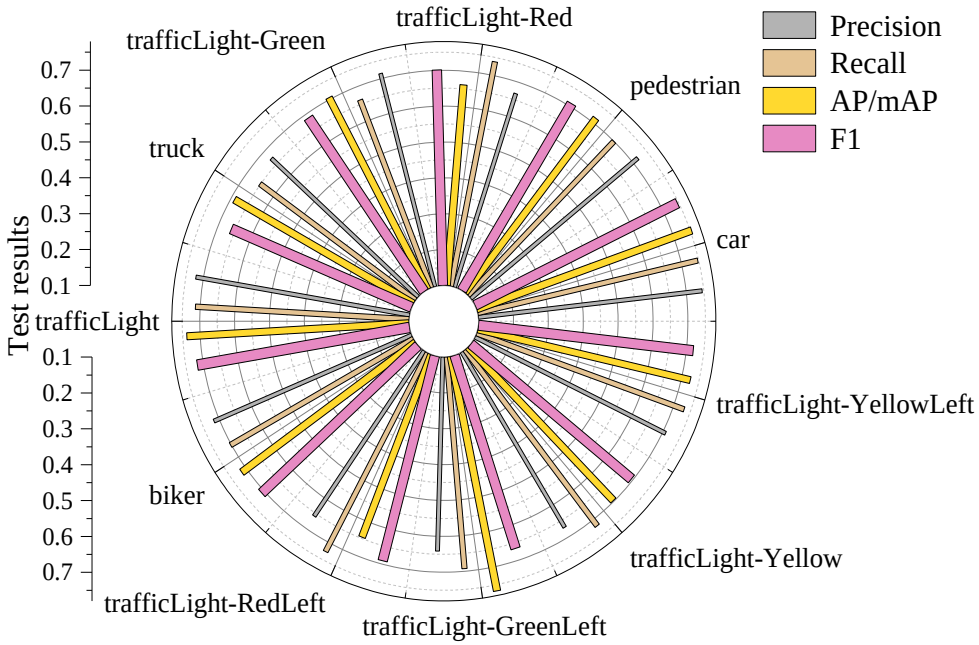

Figure 5: Different category test results in the Udacity verification set

4.2 Obstacle avoidance path planning analysis

The viability of the planned obstacle avoidance path planning control model is primarily tested using simulation experiments. On the experiment, the road setting that the inspection robot is moving on is simulated, and the map setting is simulated by the raster approach. Default size of the raster map is 20 x 20. According to the raster map, the Bug2 algorithm, A-star algorithm, RRT algorithm, APF algorithm, and the improved APF algorithm presented in this paper are applied to various situations to plan paths. The performance of path planning is measured by computing the average number of iterations, average planning time and average path lengths of all the algorithms. Comparison outcomes of the path planning algorithms are tabulated in Table 2 and the effect of the path planning in one scenario is illustrated in Fig. 6.

Based on the comparison findings, the enhanced APF algorithm presented in this paper achieves the least planning time of 4.95 ms and its mean number of iterations is 8 which is also significantly fewer than the traditional RRT algorithm. The planned path may have some redundancy in comparison with the A star algorithm and its length is 24 grids but it is not necessary that the path should be the global shortest one. With respect to the planning results depicted in the figure and the real-life use of the inspection robot, the planned route produced by the improved APF algorithm can provide more guidance and control to the robot to go around the obstacle beforehand and still make sure that the inspection robot travels on a rather safer road region.

Table 2: Comparison of path planning algorithms

Algorithm	Average iteration times	Mean planning time/ms	Mean path length/ lattice
Bug2	-	12.17	47
A*	-	15.96	20
RRT	20	10.41	38
APF	9	6.02	28
Improved APF	8	4.95	24

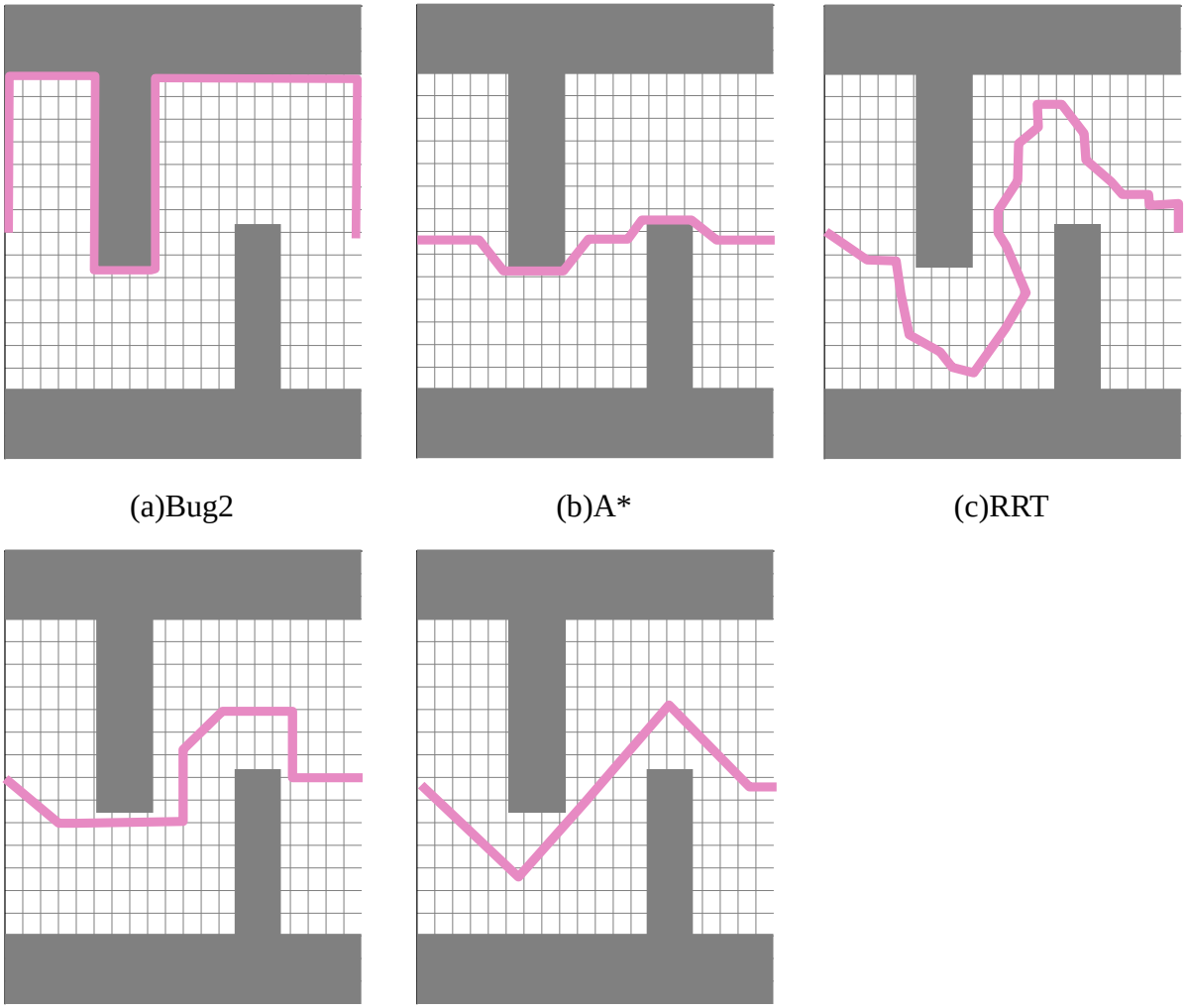

(a)Bug2 (b)A* (c)RRT

(d)APF (e)Improved APF

Figure 6: Comparison of path planning effects

4.3 Practical scenario testing

In order to further verify the practical landing effect of the proposed method, the proposed cooperative target detection algorithm and obstacle avoidance path control algorithm are transplanted to the intelligent inspection system and tested in the actual robot inspection road scene. The experiment utilizes the camera that comes with the inspection robot to obtain road environment images, and adjusts the image size to 512pixel×512pixel, from which about 3,000 images are screened for manual labeling, with a total of five types of targets (road, weeds, stones, fences, obstacles), and the cooperative target detection algorithm is trained and tested after constituting a dataset with a ratio of 7:3, and the test results are shown in Table 3. The test results are shown in Table 3, which are mainly based on the global (G), average (C), and mean-intersection-and-parallel-ratio (mIoU) accuracies to evaluate the detection effect, and on the running time per frame image (FPS) to evaluate the inspection robot navigation and obstacle avoidance control effect.

Since the actual scene dataset is relatively simpler than the public dataset, the accuracy of each target detection algorithm has been improved, and the accuracy gap between the methods has been reduced, while the method of this paper basically achieves higher performance in the actual scene in terms of accuracy and efficiency, with an FPS of 22, and

higher results in the global (G), average (C), and mean-intersection-and-union ratio (mIoU) than those of the comparison methods, which are respectively 95.07%, 85.28%, and 75.22%, effectively verifying the adaptability of the method.

Table 3: Test results for actual scenarios

Detection algorithm	*FPS*	Test accuracy/%		
		G	*C*	*mIoU*
SSD-VGG16	10	92.91	82.55	72.53
Faster R-CNN-ResNet50	13	94.68	84.73	69.94
RetinaNet-ResNet50	15	93.16	81.05	74.04
FCOS-ResNet50	16	91.78	83.55	70.84
TridentNet-ResNet50	18	92.42	82.22	73.27
CornerNet-Hourglass104	20	91.31	80.65	72.84
Ours	22	95.07	85.28	75.22

5 Conclusion

Intelligent inspection system is capable of performing equipment inspection, facility checking and security patrol operations automatically. This paper presents a cooperative target detection algorithm and an obstacle-avoidance path planning algorithm based on this system, which intends to implement collaborative decision-making and control of several intelligent agents. The key findings can be summarized in the following way:

(1) The mAP value of the cooperative target detection algorithm proposed in this paper is 0.733 on the Udacity dataset. The detection performance is enhanced by 0.6-10.2 percent relative to the comparative target detection algorithm. Besides, the detection accuracy, recall, AP/mAP, and F1 scores of 11 types of targets are between 0.63 and 0.76 which indicate that the algorithm can perform well in cooperative target detection.

(2) The improvement of APF algorithm-based obstacle avoidance path planning algorithm demonstrates the highest number of iterations (8 iterations) and the lowest planning time (4.95 ms). On average, its path length is 24 grids, which is less than the majority of comparison methods. Hence, the obstacle avoidance control of the inspection robot can be effectively implemented.

(3) During the real-scene test, the FPS of the suggested approach is 22 and the detection accuracy is the highest. The suggested method will be able to successfully sense any target obstacles within the scene that the robot is placed in, plan the navigating and avoiding obstacles path effectively, help the robot to finish the inspection mission, and facilitate cooperative decision-making and operation amongst several intelligent agents in the intelligent inspection system.

Despite the proposed approach achieving higher results, there is still a space to improve collaborative target detection accuracy and obstacle-avoidance path length. The future modifications can be done to the YOLOv3 network to increase the efficiency of target detecting network. At the same time, the obstacle-avoidance path planning algorithm may be optimized further to work in more complex situations.

About the Author

Yutian Wang was born in Ordos, Inner Mongolia, P.R. China, in 1989. He received his MSc degree in Electrical Power Engineering from the University of Southampton, UK. He is

currently working at Guoneng Guohua (Beijing) Cogeneration Power Co., Ltd., where he is mainly responsible for production management and technological innovation. In addition, he is pursuing an Engineering Doctorate at the School of Electrical Engineering, Beijing Jiaotong University, with research focusing on intelligent energy systems and smart power generation.

References

[1] Wang, F., Sun, W., Lv, S., Zhang, R., Zhang, L., & Chen, S. (2025). Research on the Application of UAV Intelligent Patrol Inspection Technology in Photovoltaic Construction Management. In Digitalization and Management Innovation III (pp. 693-700). IOS Press.

[2] Gohari, A., Ahmad, A. B., Rahim, R. B. A., Supa'at, A. S. M., Abd Razak, S., & Gismalla, M. S. M. (2022). Involvement of surveillance drones in smart cities: A systematic review. IEEE Access, 10, 56611-56628.

[3] Dorri, A., Kanhere, S. S., & Jurdak, R. (2018). Multi-agent systems: A survey. Ieee Access, 6, 28573-28593.

[4] Chen, F., & Ren, W. (2019). On the control of multi-agent systems: A survey. Foundations and Trends® in Systems and Control, 6(4), 339-499.

[5] Xie, J., & Liu, C. C. (2017). Multi-agent systems and their applications. Journal of International Council on Electrical Engineering, 7(1), 188-197.

[6] Cai, H., Su, Y., & Huang, J. (2022). Cooperative control of multi-agent systems. Cham: Springer-Verlag.

[7] Gulzar, M. M., Rizvi, S. T. H., Javed, M. Y., Munir, U., & Asif, H. (2018). Multi-agent cooperative control consensus: A comparative review. Electronics, 7(2), 22.

[8] Shi, P., & Shen, Q. (2015). Cooperative control of multi-agent systems with unknown state-dependent controlling effects. IEEE Transactions on Automation Science and Engineering, 12(3), 827-834.

[9] Han, J., Wang, C. H., & Yi, G. X. (2013, June). Cooperative control of UAV based on multi-agent system. In 2013 IEEE 8th Conference on Industrial Electronics and Applications (ICIEA) (pp. 96-101). IEEE.

[10] Xin, L., Jingjing, D., Guozhe, Z., & Lin, D. (2020, June). Research on the control problem based on multi-agent cooperation and consistency. In 2020 International Conference on Artificial Intelligence and Electromechanical Automation (AIEA) (pp. 272-275). IEEE.

[11] Zhang, Z., Liu, Y., & Yang, S. (2025). Consistent Cooperative Control of Multi-Support Systems Using Multi-Agent Reinforcement Learning With Attention Mechanism. International Journal of Robust and Nonlinear Control.

[12] Qin, J., Ma, Q., Zheng, W. X., & Gao, H. (2015, December). H∞ group consensus for

clusters of agents with model uncertainty and external disturbance. In 2015 54th IEEE conference on decision and control (CDC) (pp. 2841-2846). IEEE.

[13] ur Rehman, A., Rehan, M., Iqbal, N., & Ahn, C. K. (2020). LPV scheme for robust adaptive output feedback consensus of Lipschitz multiagents using Lipschitz nonlinear protocol. IEEE Transactions on Systems, Man, and Cybernetics: Systems, 51(11), 7040-7050.

[14] Dong, Y., & Huang, J. (2014). Leader-following connectivity preservation rendezvous of multiple double integrator systems based on position measurement only. IEEE Transactions on Automatic Control, 59(9), 2598-2603.

[15] Tran, V. P., Santoso, F., Garratt, M. A., & Anavatti, S. G. (2020). Distributed artificial neural networks-based adaptive strictly negative imaginary formation controllers for unmanned aerial vehicles in time-varying environments. IEEE Transactions on Industrial Informatics, 17(6), 3910-3919.

[16] Bao, G., Ma, L., & Yi, X. (2022). Recent advances on cooperative control of heterogeneous multi-agent systems subject to constraints: A survey. Systems Science & Control Engineering, 10(1), 539-551.

[17] Li, Z., Wu, Z., Li, Z., & Ding, Z. (2019). Distributed optimal coordination for heterogeneous linear multiagent systems with event-triggered mechanisms. IEEE Transactions on Automatic Control, 65(4), 1763-1770.

[18] Yu, J., Dong, X., Li, Q., Lü, J., & Ren, Z. (2022). Adaptive practical optimal time-varying formation tracking control for disturbed high-order multi-agent systems. IEEE Transactions on Circuits and Systems I: Regular Papers, 69(6), 2567-2578.

[19] Li, Y., Dong, S., Li, K., & Tong, S. (2023). Fuzzy adaptive fault tolerant time-varying formation control for nonholonomic multirobot systems with range constraints. IEEE Transactions on Intelligent Vehicles, 8(6), 3668-3679.

[20] Jia, Y., & Zhang, W. (2017, January). Three-dimensional leader-follower formation flocking of multi-agent system. In Pro. Int. Conf. Artif. Life. Robot. (pp. 5-8).

[21] Chen, Y., Xu, H., Dong, L., & Li, Z. (2024). Fully distributed secure observation and consensus for multi-agent systems with uncertain communication topology. ISA transactions, 145, 176-189.

[22] Zhang, S. Q., Che, W. W., & Deng, C. (2022). Observer-based event-triggered secure synchronization control for multi-agent systems under false data injection attacks. International Journal of Robust and Nonlinear Control, 32(8), 4843-4860.

[23] Sukhbaatar, S., & Fergus, R. (2016). Learning multiagent communication with backpropagation. Advances in neural information processing systems, 29.

[24] Wang, Y., Cao, J., & Kashkynbayev, A. (2023). Multi-agent bifurcation consensus-based multi-layer UAVs formation keeping control and its visual simulation. IEEE Transactions on Circuits and Systems I: Regular Papers, 70(8), 3221-3233.

[25] Yang, X., Hu, J., Tan, C., & Yi, X. (2024). Prediction-based scaled consensus control for heterogeneous multi-agent systems under switching topologies. Nonlinear Dynamics, 112(6), 4529-4550.

[26] Feng, Z., Sun, C., & Hu, G. (2016). Robust connectivity preserving rendezvous of multirobot systems under unknown dynamics and disturbances. IEEE transactions on control of network systems, 4(4), 725-735.

[27] Sun, L., Zhang, H., Xu, W., & Tomizuka, M. (2023). Efficient multi-task and transfer reinforcement learning with parameter-compositional framework. IEEE Robotics and Automation Letters, 8(8), 4569-4576.

[28] Chen, C., Lewis, F. L., Xie, K., Lyu, Y., & Xie, S. (2023). Distributed output data-driven optimal robust synchronization of heterogeneous multi-agent systems. Automatica, 153, 111030.

[29] Van Der Pol, E. (2016). Deep reinforcement learning for coordination in traffic light control. Master's thesis, University of Amsterdam.

[30] Foerster, J., Farquhar, G., Afouras, T., Nardelli, N., & Whiteson, S. (2018, April). Counterfactual multi-agent policy gradients. In Proceedings of the AAAI conference on artificial intelligence (Vol. 32, No. 1).

[31] Hu, S., Zhu, F., Chang, X., & Liang, X. (2021). Updet: Universal multi-agent reinforcement learning via policy decoupling with transformers. arXiv preprint arXiv:2101.08001.

[32] Lowe, R., Wu, Y. I., Tamar, A., Harb, J., Pieter Abbeel, O., & Mordatch, I. (2017). Multi-agent actor-critic for mixed cooperative-competitive environments. Advances in neural information processing systems, 30.

[33] Setter, T., & Egerstedt, M. (2016). Energy-constrained coordination of multi-robot teams. IEEE Transactions on Control Systems Technology, 25(4), 1257-1263.

[34] Shen, Z., Dong, T., & Huang, T. (2025). Data-driven bipartite synchronization control of multi-agent systems with asymmetric input saturation over switching networks. Applied Mathematics and Computation, 494, 129280.

[35] Fei, Y., Shi, P., & Lim, C. C. (2022). Neural-based formation control of uncertain multi-agent systems with actuator saturation. Nonlinear Dynamics, 108(4), 3693-3709.